Experimental and Theoretical Study of the Surface-Controlled Dissolution of Cylindrical Particles. Application to Solubilization of Potassium Hydrogen Carbonate in Hot Dimethylformamide

Claire L. Forryan,[†] Oleksiy V. Klymenko,[†,§] Shelley J. Wilkins,[†,||] Colin M. Brennan,[‡] and Richard G. Compton*,[†]

Physical and Theoretical Chemistry Laboratory, University of Oxford, South Parks Road, Oxford, OX1 3QZ, U.K., and Syngenta, Leeds Road, Huddersfield, HD2 1FF, U.K.

Received: June 22, 2005

In this paper we present a mathematical model for the surface-controlled dissolution of cylindrical solid particles. This is employed to interpret experimental data published previously for the dissolution of potassium bicarbonate in dimethylformamide at elevated temperatures. Significant kinetic differences in assuming cylindrical rather than spherical shapes are reported with the former representing a closer approximation to the true shape of the particles as revealed by scanning electron microscopy. From the fits of experimental data to the cylindrical model for the surface-controlled dissolution, the dissolution rate constant, *k*, for the dissolution of $KHCO_3$ in DMF was found to be $(9.6 \pm 1.6) \times 10^{-9}$ mol cm^{-2} s^{-1} at 100 °C, and the activation energy for the dissolution was 34.5 kJ mol^{-1} over the temperature range of 60−100 °C. Comparison between cylindrical and spherical dissolution theory highlights the importance of considering the particle shapes for realistic modeling of surface-controlled dissolution kinetics.

1. Introduction

Understanding the dissolution kinetics of solid particles is important in natural processes and in industry,[1−13] particularly in the development and operation of processes for the production of agrochemicals and pharmaceuticals. Reactions at the solid−liquid interface may occur via several mechanisms; the focus of our studies being where the rate-determining step involves the dissolution of the solid substrate.[14] Surprisingly, although heterogeneous systems are used widely in the production of fine chemicals, there is little literature information on the dissolution of solid particles in organic solvents. Formerly, studies of the dissolutions of inorganic solids have been in aqueous solutions,[7,12,13,15,16] such as the dissolution of limestone in aqueous electrolyte,[12,17−20] and only particles of sizes in a small diameter fraction or single crystals have been selected.

The use of a strong inorganic base (e.g., potassium and sodium carbonates or potassium and sodium hydroxides) in an organic solvent (e.g., dimethylformamide, acetonitrile, or dimethyl sulfoxide) is often used to facilitate the formation of a required anionic organic nucleophile in many organic processes, such as epoxide synthesis from sulfur ylides,[21,22] synthesis of primary amines,[23,24] reduction of allylic nitro compounds to oximes,[23] and several alkylations.[22,25,26] Custers et al.[25] examined the trialkylation of methyl gallate, where the reaction times appeared to be a function of particle size distribution of the base, potassium carbonate. Previous papers have investigated the surface-controlled dissolution of both potassium bicarbonate[27] and potassium carbonate[28] in DMF at elevated temperatures in the presence of ultrasound. We followed the dissolution experimentally via the homogeneous deprotonation of 2-cyanophenol by dissolved solid (Scheme 1); the loss of 2-cyanophenol was detected electrochemically, and the formation of the 2-cyanophenolate anion was monitored via UV/visible spectroscopy. Theory was developed for the surface-controlled dissolution of solid particles over time as a function of the particle distribution of the solid.[27] In the kinetic treatment, we considered that after being placed into the solution the particles start to dissolve with the rate constant, *k*. The rate of change of the number of moles of the species in a particle being proportional to the rate constant, *k*, and the particle surface area, assuming that the particles are spherical. From the evaluation over all values of particle diameter, we obtained the time dependence of the total number of moles of the species in the particle mixture. This was illustrated effectively for the dissolution of both inorganic solids, and values for the dissolution rate constant, *k*, were determined.

SCHEME 1: Deprotonation of $KHCO_3$ with 2-Cyanophenol in DMF

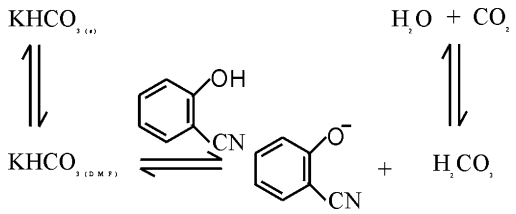

In this paper we present a theory for the surface-controlled dissolution of cylindrical solid particles over time. This is compared to that for spherical-shaped particles in order to show the influence of particle shape on the dissolution kinetics of a

* To whom correspondence should be addressed. Tel: +44-01865-275413. Fax: +44-01865-275410. E-mail: richard.compton@chemistry.ox.ac.uk.

† University of Oxford.

‡ Syngenta.

§ Now at: Mathematical and Computer Laboratory, Kharkov National University of Radioelectronics, 14 Lenin Avenue, Kharkov 61166, Ukraine.

|| Now at: Department of Materials, University of Oxford, Parks Road, Oxford, OX1 3PH, United Kingdom.

10.1021/jp058197a CCC: $30.25
Published on Web 10/19/2005

solid. The model is then used to reexamine the data published previously on the dissolution kinetics of $KHCO_3$ in DMF at elevated temperatures because scanning electron microscopy of the solid revealed that the comprising particles of the solid are more cylindrical in shape. The results give an improved fit of experimental to theoretical data, from which a refined value for the dissolution rate constant, k, of $KHCO_3$ in DMF is determined. We also model the dissolution in DMF of another sample of $KHCO_3$ successfully, which is composed of cylindrical particles having a different size distribution.

2. Experimental Section

2.1. Chemical Reagents. All experiments were carried out in *N*,*N*-dimethylformamide (DMF, Aldrich, 99.9 +%, HPLC grade). The DMF was treated carefully by drying over Linde 5-Å molecular sieves (Aldrich) for a minimum of 48 h. Prior to use it was shaken with ICN alumina N-super 1 (ICN Biomedicals GmbH, Germany), and the solvent was decanted off. The water content of the solvent was determined by Karl−Fischer titration (Metrohm, 758 KFD Titrino),[29] and it was found that the DMF drying procedure outlined above yielded DMF with a water content of ca. 0.04 wt % (2.3×10^{-2} mol L^{-1}), compared to DMF as supplied, which has a water content of ca. 0.15 wt % (8.6×10^{-2} mol L^{-1}).

2-cyanophenol (Aldrich) and potassium bicarbonate (Aldrich) were obtained of the highest commercially available grade and used without further purification. Syngenta (Huddersfield, U.K.) supplied a second sample of potassium bicarbonate.

2.2. Instrumentation. *2.2.2. High-Temperature and Ultrasound Apparatus.* The ultrasonic generator used was a model VCX 5000 (Sonics and Materials, USA) horn equipped with a 3-mm-diameter titanium microtip emitting 25 kHz ultrasound. The power output of the transducer was calculated calorimetrically in DMF[30,31] for which an amplitude of 5% was found to correspond to 8 W cm^{-2} and employed for all experiments.

The high-temperature experiments were carried out in a cell with a solution volume of 15 cm^3 by hot air circulation from an electronically controlled heat gun within a small box of insulating material with a front glass wall.[32] A Pt resistance thermometer controlled the air temperature, and a thermocouple in contact with the solution was used to read the temperature. The ultrasound horn was inserted from above into the cell through a precision bore aperture in the Teflon cell lid, which was manufactured in house to minimize heat losses. Temperature control was most important, and care was taken to ensure that all experiments were carried out at the required temperatures to ±1 °C. To maintain the solution temperatures of 60, 80, 90, or 100 °C under the application of the power ultrasound, external heating required hot air circulation of ca. 55, 65, 80, and 86 °C, respectively.

The solutions of $KHCO_3$ in DMF were heated under ultrasound at elevated temperatures for a 1−2 h time period before the addition of 2-cyanophenol. The solutions were degassed thoroughly with nitrogen (BOC gases) throughout their initial heating, and a continuous flow of nitrogen over the solution was maintained throughout the experiments to ensure that no oxygen was in contact.

2.2.3. UV/Visible Spectroscopy. UV/visible spectra were recorded on a Unicam UV2 series UV/visible spectrophotometer (Unicam, Cambridge, U.K.) using a quartz cuvette of 1-cm path length, scanning over a wavelength of 275−400 nm. Small volume samples (ca. 50 μl) were removed at regular time intervals from the ultrasound-heated solutions, over a 1 h period, and allowed to cool to room temperature. These were diluted with DMF by a known factor, and their UV/visible spectra were recorded. Each spectrum was background subtracted from that of blank DMF.

2.2.4. Scanning Electron Microscopy. Scanning electron microscopy (SEM) images were recorded using a JEOL 6500F instrument.

3. Theory

3.1. Surface-Controlled Dissolution of Cylindrical Solid Particles. In the kinetic treatment that follows, we consider the rate of dissolution of solid particles by modeling the number of moles of solid remaining undissolved in solution over time.

Let us consider a sample of cylindrical particles of mass m and density ρ, initially with the circular end having diameter d_0 and cylindrical length l_0. As the particle dissolves, the diameter and cylindrical length are denoted l and d, respectively, where $l = zd$ and $l_0 = z_0 d_0$. Hence

$$\text{volume} = \frac{\pi}{4} d^2 l \tag{1}$$

and the number of moles of species in this particle is

$$n = \frac{\pi\rho}{4M} d^2 l \tag{2}$$

From eq 1

$$\frac{\mathrm{d}n}{\mathrm{d}t} = \frac{\pi\rho}{4M}\left[2dl\frac{\mathrm{d}d}{\mathrm{d}t} + d^2\frac{\mathrm{d}l}{\mathrm{d}t}\right] \tag{3}$$

After being placed into the solution, the particles start to dissolve with the rate constant k. The rate of change of the number of moles of the species in a particle is proportional to the rate constant, k, and the particle surface area, $S = \pi dl + (\pi/2)d^2$. Hence, the following differential equation can be written for a single particle of diameter d

$$\frac{\mathrm{d}n}{\mathrm{d}t} = -kS = -k\left[\pi dl + \frac{\pi}{2} d^2\right] \tag{4}$$

From comparison of eqs 3 and 4

$$\frac{\pi\rho}{4M} 2dl\frac{\mathrm{d}d}{\mathrm{d}t} = -k\pi dl$$

Therefore

$$\frac{\mathrm{d}d}{\mathrm{d}t} = -\frac{2Mk}{\rho} \tag{5}$$

and

$$\frac{\pi\rho}{4M} d^2\frac{\mathrm{d}l}{\mathrm{d}t} = -\frac{k\pi}{2} d^2$$

Therefore

$$\frac{\mathrm{d}l}{\mathrm{d}t} = -\frac{2Mk}{\rho} \tag{6}$$

Both dimensions of the cylinder shrink at the same rate. Integrating eqs 5 and 6

$$d = d_0 - \frac{2Mk}{\rho} t \tag{7}$$

$$l = l_0 - \frac{2Mk}{\rho} t \tag{8}$$

Therefore

$$z(t) = \frac{d}{l} = \frac{l_0 - \frac{2Mk}{\rho}t}{d_0 - \frac{2Mk}{\rho}t} \tag{9}$$

Dissolution is complete when the cylinder diameter or its length becomes zero, whichever happens sooner, that is, at

$$t = \frac{d_0\rho}{2Mk} \text{ or } t = \frac{l_0\rho}{2Mk}$$

whichever is smaller. Returning to eq 3

$$n(t, d_0, l_0) = \frac{\pi\rho}{4M}\left(d_0 - \frac{2Mk}{\rho}t\right)^2\left(l_0 - \frac{2Mk}{\rho}t\right) \tag{10}$$

As an aside, note that z is a constant only when

$$z_0 = \frac{l_0 - \frac{2Mk}{\rho}t}{d_0 - \frac{2Mk}{\rho}t}$$

therefore, when $l_0 = d_0$, z_0 is equal to one, otherwise z varies throughout the experiment. In particular, if $l_0 < d_0$ then the ratio of particle length to its diameter, z, will decrease steadily to zero, whereas if $l_0 > d_0$ then this ratio will increase to infinity.

Equation 10 gives negative values for $t > (d_0, 0)\rho/2Mk$ or $t > (l_0, 0)\rho/2Mk$, that is, after a particle has been fully dissolved. Making use of the Heaviside step function, we can rewrite eq 10 as

$$n_1(t, d_0, l_0) = \frac{\pi\rho}{4M}\left(d_0 - \frac{2Mk}{\rho}t\right)^2\left(l_0 - \frac{2Mk}{\rho}t\right) H\left(\frac{d_0\rho}{2Mk} - t\right) H\left(\frac{l_0\rho}{2Mk} - t\right) \tag{11}$$

which is now correct for all values of t.

Next we can evaluate eq 11 for different particle size distributions to obtain the time dependence of the number of moles of the solid in solution. For a monodispersed solid of starting mass m, of which all cylindrical particles have the same initial diameter, d_0, and initial cylindrical length of l_0, where $l_0 = zd_0$

$$n(t) = \frac{m}{\pi d^2 l}\left(d - \frac{2Mk}{\rho}t\right)^2\left(l - \frac{2Mk}{\rho}t\right) \tag{12}$$

Considering now that the sample of particles is described by a number distribution function $f(d)$, and assuming that all cylindrical particles have the same initial z_0 value, the number of particles with d_0 and z_0 is given by

$$\mathrm{d}N(d_0, z_0) = f(d_0)\,\mathrm{d}d_0 \tag{13}$$

and hence

$$\mathrm{d}n(d_0, z_0, t) = n_1(d_0, z_0, t)\,\mathrm{d}N(d_0) = \frac{\pi\rho}{4M}\left(d_0 - \frac{2Mk}{\rho}t\right)^2\left(z_0 d_0 - \frac{2Mk}{\rho}t\right) H\left(\frac{d_0\rho}{2Mk} - t\right) H\left(\frac{z_0 d_0\rho}{2Mk} - t\right) f(d_0)\,\mathrm{d}d_0 \tag{14}$$

Integrating eq 13 over all values of particles, we obtain the time dependence of the total number of moles of the species in the particle mixture

$$n(t) = \frac{\pi\rho}{4M}\int_0^\infty \left(d_0 - \frac{2Mk}{\rho}t\right)^2\left(z_0 d_0 - \frac{2Mk}{\rho}t\right) H\left(\frac{d_0\rho}{2Mk} - t\right) H\left(\frac{z_0 d_0\rho}{2Mk} - t\right) f(d_0)\,\mathrm{d}d_0 \tag{15}$$

Elimination of the Heaviside function from the integral gives the final result in the form

$$n(t) = \frac{\pi\rho}{4M}\int_{\frac{2Mk}{\rho}t\left(H(z_0-1)+\frac{1}{z_0}H(1-z_0)\right)}^\infty \left(d_0 - \frac{2Mk}{\rho}t\right)^2\left(z_0 d_0 - \frac{2Mk}{\rho}t\right) f(d_0)\,\mathrm{d}d_0 \tag{16}$$

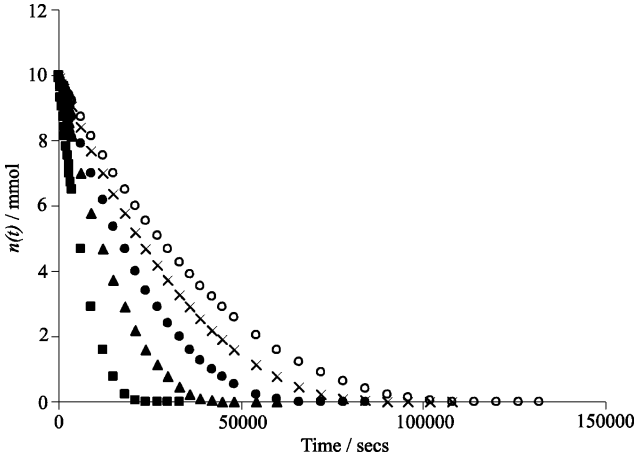

Figure 1. Plots of $n(t)$/mmol against time/s for the dissolution of 1.0 g $KHCO_3$ containing cylindrical monodispersed particles of diameter (■) 200, (▲) 400, (●) 600, (×) 800, and (○) 1000 μm and $z_0 = 2$.

3.2. Theoretical Results. The theory presented above was investigated for the dissolution of a solid having monodispersed cylindrical particles and compared to that developed from previous theory for the dissolution of spherical particles in solution. In each case the model is tested for a 1.0 g starting mass of solid, with k, the dissolution rate constant, having a value of 9.6×10^{-9} mol cm^{-2} s^{-1}, corresponding to that determined below for the dissolution of $KHCO_3$ in DMF at 100 °C.

The dissolution with time was modeled for samples containing cylindrical particles of diameter 200, 400, 600, 800, and 1000 μm, and $z_0 = 2$ for all particles. The resulting curves of the number of moles of $KHCO_3$ undissolved/$n(t)$, against time are given in Figure 1. As expected, the smaller the particle size, the more quickly they dissolve. There is a fixed starting mass of solid; therefore, as the volume and mass of the particles increase, the number of particles in the sample decreases. For the cylindrical diameters of 200, 400, 600, 800, and 1000 μm, the number of particles in the 1.0-g sample are approximately 3.7×10^4, 4.6×10^3, 1.4×10^3, 5.7×10^2, and 2.9×10^2, respectively.

The effect of varying the initial value of z and hence the cylindrical length, l_0, was examined for particles having the same initial diameter of 200 μm and increasing z_0 values of 1, 2, 4, and 8, hence l_0 being 200, 400, 800, and 1600 μm, respectively. The initial number of particles in each sample is 7.4×10^4, 3.7×10^4, 1.8×10^4, and 9.2×10^3, respectively. Figure 2 shows that, as expected, as the particle size increases the dissolution slows. The decrease in l_0 of the cylinders does not speed up the

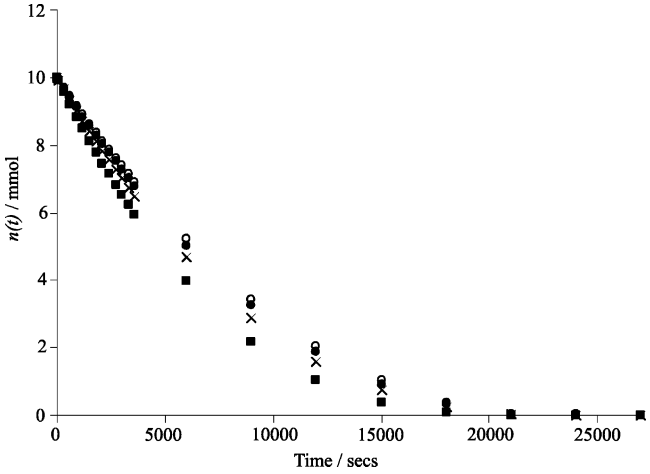

Figure 2. Plots of $n(t)$/mmol against time/s for the dissolution of 1.0 g $KHCO_3$ containing cylindrical monodispersed particles with initial diameter of 200 μm and z_0 values of (■) 1, (×) 2, (●) 4, and (○) 8.

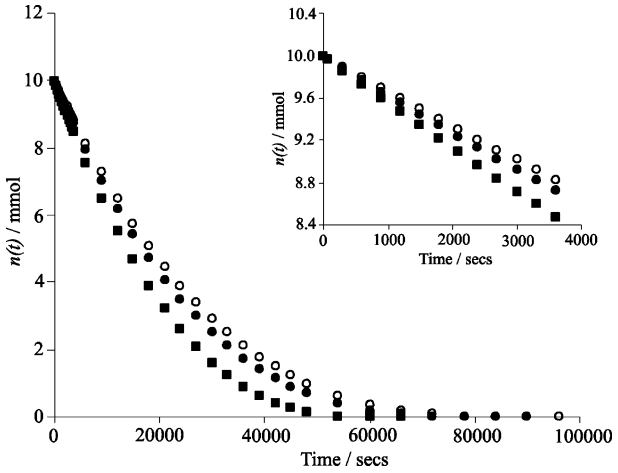

Figure 3. Plots of $n(t)$/mmol against time/s for the dissolution of 1.0 g $KHCO_3$ containing (■) cylindrical monodispersed particles with an initial diameter of 500 μm and $z_0 = 2$, compared to monodiespersed spherical particles of equal (●) volume and (○) surface area. The inset shows the enlarged portions of the graph for 0−4000 s.

dissolution of the particles to as great an extent as decreases in d_0 seen in the previous figure. The volume of the particles is proportional to the cylinder length and to the square of the diameter. Consequently, changes in d have a greater influence on the particle size and thus the number of particles in the solid. The dissolution is complete when the cylinder diameter or length becomes zero; hence, as both dimensions of the cylinder shrink with the same rate and for the $KHCO_3$ particles $l_0 \geq d_0$, this occurs when d becomes zero. Therefore, theory would predict that for the samples of $KHCO_3$ particles above that possess different z_0 values, complete dissolution of the solid will occur after the same time in each case because of the same d_0 of all particles.

Now we can compare the dissolution of cylindrical particles to that of spherical particles. The theory for the surface-controlled dissolution of spherical particles is detailed in a previous paper.[27] Consider a sample of inorganic solid composed of monodispersed cylindrical particles with $d_0 = 500$ μm and $z_0 = 2$; hence, each particle has a volume of 1.96×10^{-4} cm^3 and a surface area of 1.96×10^{-2} cm^2. Figure 3 shows the comparison to the dissolution of monodispersed spherical particles, also with $k = 9.6 \times 10^{-9}$ mol cm^{-2} s^{-1}, for each particle having (●) the same volume (initial particle diameter of 721 μm) and (○) the same surface area (initial particle diameter of 790 μm). The inset of Figure 3 corresponds to the enlargement of the curves for the initial loss of solid. In each case it can be seen that the cylindrical particles dissolve faster than the spheres. The initial number of both the cylindrical particles and the spherical particles with the same volume is 2.3×10^3 in the fixed mass samples. The initial number of the spherical particles with the same surface area as but larger volumes than those of the cylinders is 1.8×10^3. The cylinders have a much larger surface-to-volume ratio compared to that of the spheres, hence giving a faster loss of solid into solution. Complete dissolution of the cylinders, spheres with equal volume, and spheres with equal surface area is attained after times of approximately 56 000, 84 000, and 90 000 s, respectively, corresponding to a decrease in the surface-to-volume ratio of the particles. Therefore, when modeling the surface-controlled dissolution of solid particles it is essential to identify the shapes of the individual particles correctly.

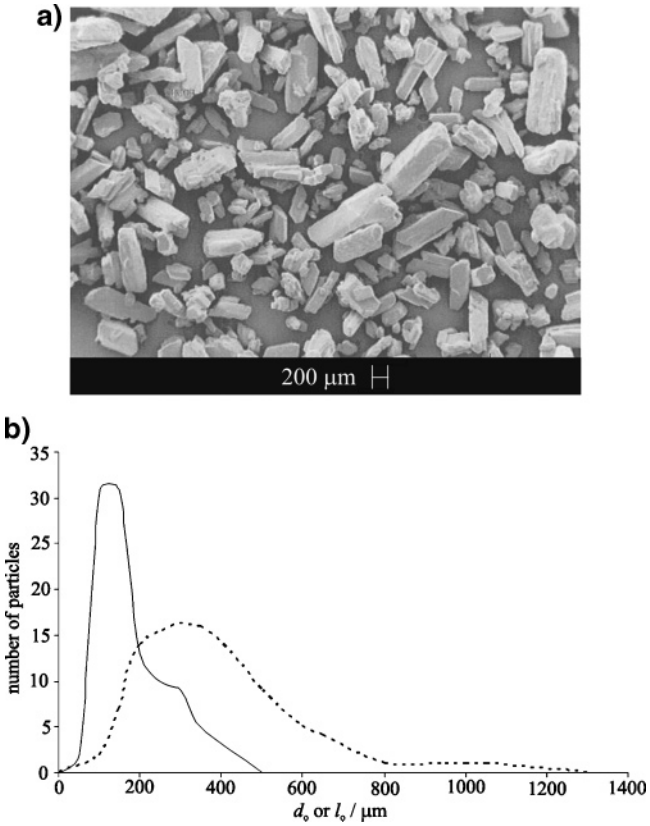

Figure 4. (a) SEM image of $KHCO_3$ and (b) number distribution functions, $f(d)$ (−) and $f(l)$ (-·-·-·-·-), of the cylindrical particle dimensions for the $KHCO_3$ sample.

4. Results and Discussion

4.1. Scanning Electron Microscopy Imaging of $KHCO_3$. Figure 4a displays an SEM image for a sample of the $KHCO_3$ used in the previous experiments.[27] It can be seen that the individual $KHCO_3$ particles are rod-like in shape; hence, a cylindrical approximation is more valid. A large number of particles in the images were examined, and the cylindrical dimensions, d and l, of individual $KHCO_3$ particles were measured. Statistical analysis yielded the number mean cylindrical particle diameter $d = 170 \pm 74$ μm, cylindrical length $l = 390 \pm 196$ μm, and a mean z value of 2.4 ± 0.9. The number distribution functions, $f(d)$ and $f(l)$, given in Figure 4b for the $KHCO_3$ sample were developed from the SEM images. Figure

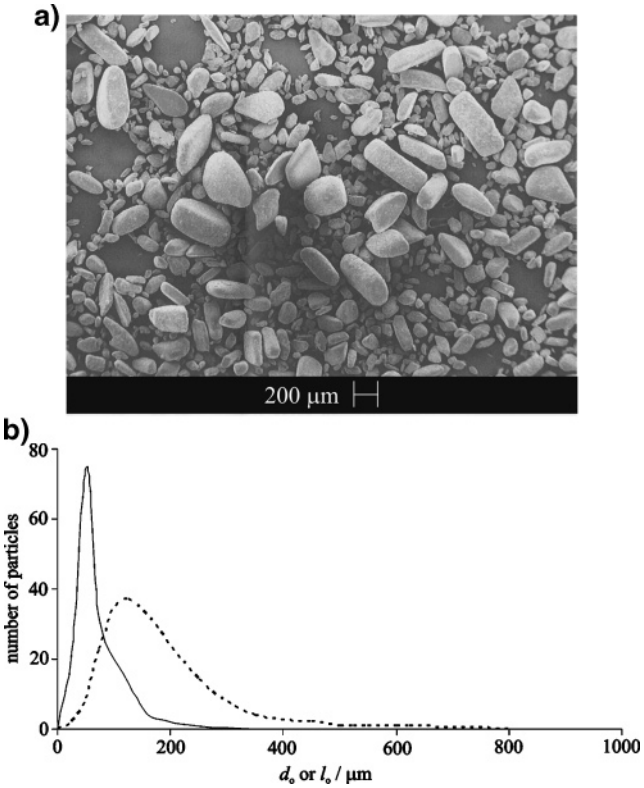

Figure 5. (a) SEM image of $KHCO_3$* and (b) number distribution functions, $f(d)$ (−) and $f(l)$ (-•-•-•-•-•-), of the cylindrical particle dimensions for the $KHCO_3$* sample.

5a shows an SEM image for a second sample of $KHCO_3$ (to be denoted $KHCO_3$*) used experimentally in this paper, which contains cylindrical-shaped particles. Inspection of the images gave the mean values of $d = 68 \pm 36$ μm, cylindrical length $l = 172 \pm 106$ μm, $z = 2.6 \pm 0.9$, and distribution functions $f(d)$ and $f(l)$ in Figure 5b.

4.2. Dissolution of Cylindrical $KHCO_3$ Particles in DMF. The dissolution of $KHCO_3$ in DMF at elevated temperatures was followed by employing a strategy reported previously, whereby the dissolved solid deprotonates the 2-cyanophenol to produce the 2-cyanophenolate anion that is detected spectroscopically.[27,28] The absorption peak of 2-cyanophenolate occurs at a wavelength of 358 nm with an absorbance of 0.764 mol^2 dm^{-6},[33] and it was analyzed over time after the addition of 2-cyanophenol to $KHCO_3$/DMF solutions at elevated temperatures. The concentration of 2-cyanophenolate formed at each reaction time was determined from the Beer−Lambert Law,[34] and taking a 1:1 mole ratio of 2-cyanophenolate produced to $KHCO_3$ reacted (Scheme 1), the number of moles of $KHCO_3$ remaining in solution at each time was calculated.

4.2.1. Determination of the Dissolution Rate Constant, k. The UV/visible spectroscopic results are analyzed using the model developed above for the surface-controlled dissolution of the cylindrical particles model. Equation 16 was solved numerically to develop plots of the number of moles of undissolved solid, $n(t)$/mol against time/s to compare the cylinder theory with experiment. The following parameters were used: mass of the inorganic solid/g, density of the solid/g cm^{-3}, molecular weight of the solid/g mol^{-1}, time/s, k/mol cm^{-2} s^{-1}, cylindrical particle diameter number distribution function, $f(d)$, (Figure 4b) with all particles having the same initial z_0 of 2.4. It has been found electrochemically and spectroscopically that initially the 2-cyanophenol deprotonation is via predissolved $KHCO_3$ in the DMF solution, followed over longer time by the slower surface-controlled dissolution of solid.[27] Hence, the mass of solid used was calculated via subtraction of the mass predissolved in solution from the initial mass of solid added and the first minute of reaction not included in the fits.

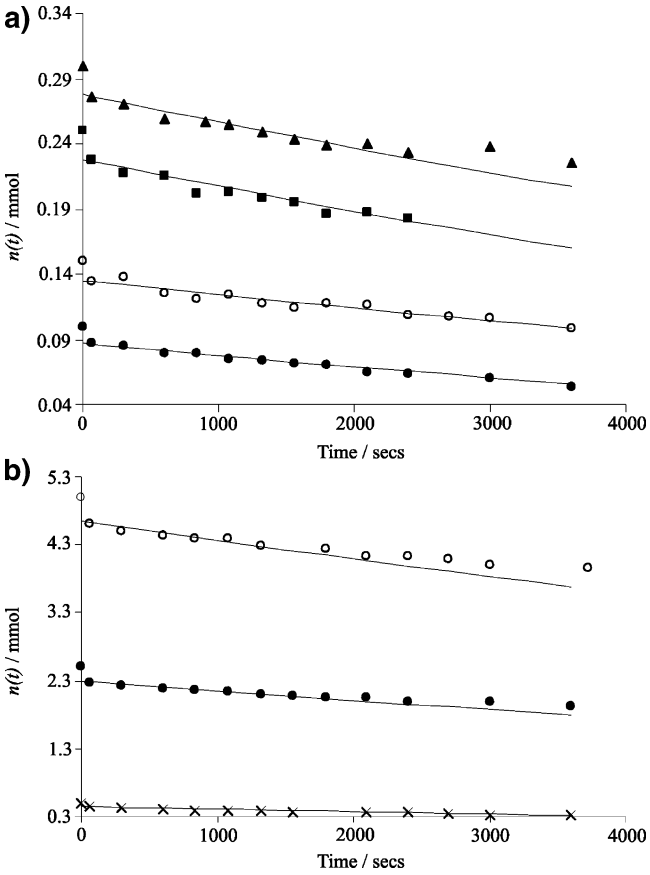

Figure 6. Plots of $n(t)$/mmol against time/s of theoretical results from the cylinder model (−) and UV/visible spectroscopic experimental results at 100 °C for the dissolution-rate-controlled process for (a) the addition of 5 mM 2-cyanophenol to (●) 0.010 g $KHCO_3$, (○) 0.015 g $KHCO_3$, (■) 0.025 g $KHCO_3$, and (▲) 0.030 g $KHCO_3$ and (b) (×) 0.050 g $KHCO_3$, 10 mM 2-cyanophenol, (●) 0.250 g $KHCO_3$, 50 mM 2-cyanophenol, and (○) 0.500 g $KHCO_3$, 100 mM 2-cyanophenol.

The dissolution of $KHCO_3$ in DMF at 100 °C was followed for $KHCO_3$ masses of 0.010, 0.015, 0.025, and 0.030 g with the addition of 5 mM 2-cyanophenol. The corresponding plots of $n(t)$ against time are given in Figure 6a. Overlaid are the theoretical fits from the cylinder model, and good fit to the experimental data can be seen. It should be noted that for the 0.030 g addition the theoretical fit does not bisect the last two experimental data points because all of the 2-cyanophenol added has been completely deprotonated, and, hence, no further 2-cyanophenolate can be generated form dissolved $KHCO_3$. Next, the additions of varying concentrations of 2-cyanophenol were investigated over the range of 1 mM to 100 mM at 100 °C to confirm that the dissolution rate constant is independent of the initial concentration of 2-cyanphenol added and initial mass of $KHCO_3$ present. Figure 6b shows the experimental and theoretical fits for solutions of DMF with $KHCO_3$ of masses 0.050, 0.250, and 0.500 g heated under ultrasound at 100 °C, with the addition of 10, 50, and 100 mM 2-cyanophenol, respectively. Again, there is good correlation between theory and experiment, hence supporting the dissolution model for cylindrical particles. The mean value determined for the dissolution rate constant, k, for the dissolution of $KHCO_3$ in DMF at 100 °C is $(9.6 \pm 1.6) \times 10^{-9}$ mol cm^{-2} s^{-1}.

TABLE 1: Values of the Dissolution Rate Controlled Constant, *k*, of $KHCO_3$ in DMF at 100 °C Determined for Cylindrical Particles Compared to those Published Previously for Spherical Particles

		all particles with size distribution $f(d)$		monodispersion of average-sized particles	
[2-cyanophenol] mM	$KHCO_3$ mass/g	cylinders[a] k/mol cm^{-2}s^{-1}	spheres[b] k/mol cm^{-2}s^{-1}	cylinders[c] k/mol cm^{-2}s^{-1}	spheres[d] k/mol cm^{-2}s^{-1}
5	0.010	1.4×10^{-8}	2.0×10^{-8}	7.8×10^{-9}	2.8×10^{-8}
5	0.015	9.0×10^{-9}	1.4×10^{-8}	6.2×10^{-9}	2.1×10^{-8}
5	0.020	8.6×10^{-9}	1.1×10^{-8}	5.8×10^{-9}	1.9×10^{-8}
5	0.025	1.1×10^{-8}	1.5×10^{-8}	7.0×10^{-9}	2.2×10^{-8}
5	0.030	8.9×10^{-9}	1.2×10^{-8}	5.9×10^{-9}	2.0×10^{-8}
5	0.035	8.9×10^{-9}	1.1×10^{-8}	6.0×10^{-9}	1.9×10^{-8}
10	0.050	1.0×10^{-8}	1.6×10^{-8}	7.2×10^{-9}	2.5×10^{-8}
50	0.250	8.5×10^{-9}	8.4×10^{-9}	5.0×10^{-9}	1.4×10^{-8}
100	0.500	8.1×10^{-9}	7.5×10^{-9}	4.6×10^{-9}	1.2×10^{-8}
	mean	9.6×10^{-9}	1.3×10^{-8}	6.2×10^{-9}	2.0×10^{-8}
	SD	1.6×10^{-9}	4.0×10^{-9}	1.0×10^{-9}	4.7×10^{-9}

[a] Values deduced using eq 16, in which $f(d)$ is that given in figure 4b. [b] Values reported in ref 27. [c] Values deduced using eq 12, in which $d_0 = 17$ μm and $l_0 = 390$ μm. [d] Values deduced using eq 10 reported in ref 27.

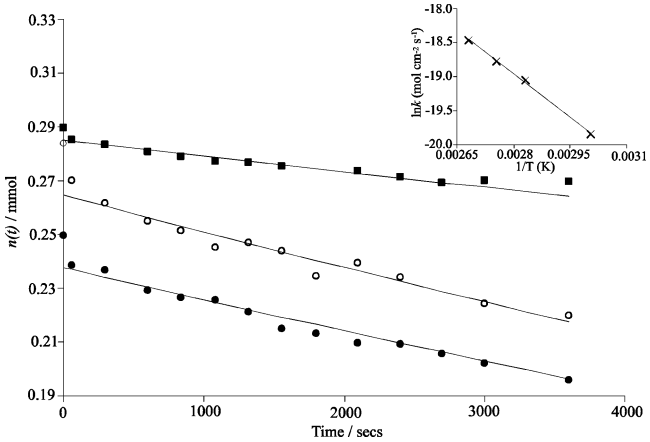

Figure 7. Plots of $n(t)$/mmol against time/s of theoretical results from the cylinder model (−) and UV/visible spectroscopic experimental results for the addition of 5 mM 2-cyanophenol to (■) 0.029 g $KHCO_3$ in DMF at 60 °C, (●) 0.025 g $KHCO_3$ in DMF at 80 °C, and (○) 0.029 g $KHCO_3$ in DMF at 90 °C. The inset shows a graph of ln(k/mol cm^{-2} s^{-1}) against 1/(T/K) over the temperature range of 60−100 °C.

The effect of temperature on the dissolution-rate-controlled constant for $KHCO_3$ in DMF was examined. The addition of 5 mM 2-cyanophenol to solutions of 0.029 g $KHCO_3$/DMF at 60 and 90 °C, and 0.025 g $KHCO_3$/DMF at 80 °C are detailed in Figure 7. The successful fits to the theoretical model are overlaid from which the values of k are found to be $(2.4 \pm 0.1) \times 10^{-9}$ mol cm^{-2} s^{-1} at 60 °C, $(5.1 \pm 0.5) \times 10^{-9}$ mol cm^{-2} s^{-1} at 80 °C, and $(7.0 \pm 0.2) \times 10^{-9}$ mol cm^{-2} s^{-1} at 90 °C. A graph of ln k against 1/T over the temperature range of 60−100 °C studies (inset of Figure 7) yields a straight line with an R^2 value of 0.999. From analysis in terms of an Arrhenius-type relation, the dissolution of $KHCO_3$ in DMF was calculated to be 34.8 ± 0.2 kJ mol^{-1}.

4.2.2. Comparison with Spherical Model. Table 1 gives the values of k determined above from all fits of experimental data at 100 °C to the cylindrical model theory, incorporating the number distribution function, $f(d)$, for the cylindrical diameter of all particles in the $KHCO_3$ sample. These are compared to those published previously from the fits of experiment to spherical particle theory, taking a spherical diameter distribution function of the whole sample as determined from particle sizing methods.[27] Also included in the table are the values of k calculated from the assumption that the $KHCO_3$ sample is a monodispersion of cylindrical or spherical particles; the solid is composed of either cylindrical particles having the mean initial dimensions of $d_0 = 170$ μm and $l_0 = 390$ μm (found from SEM images) or spherical particles all having the mean initial spherical diameter (determined using particle sizing instrumentation).

The values of k calculated from the incorporation of the size distribution function of all particles for both cylindrical and spherical theory give broadly similar values; 9.6×10^{-9} and 13.0×10^{-9} mol cm^{-2} s^{-1}, respectively. However, the standard deviations from the mean values of k are 1.6×10^{-9} and 4.1×10^{-9} mol cm^{-2} s^{-1} for cylinders and spheres, respectively. This shows the assumption that the $KHCO_3$ sample is composed of cylindrical-shaped particles gives an improved fit of the theory over all experimental dissolutions. Thus, for the surface-controlled dissolution of solid particles it is important to have knowledge of the particle shapes that comprise the solid in order to model the observed kinetics accurately.

It can be observed from Table 1 that the values of k assuming the solid is a monodispersion of average-sized particles differ from those taking the full size distributions of the solid under each experimental condition. The mean values of k determined are $(6.2 \pm 1.0) \times 10^{-9}$ mol cm^{-2} s^{-1} and $(2.0 \pm 0.5) \times 10^{-8}$ mol cm^{-2} s^{-1} for cylinders and spheres, respectively. Hence, this assumption can provide an approximation to the order of magnitude of the dissolution rate constant, but for realism and precision the shapes and size distribution of the solid particles must be known.

4.2.3. Changes in Cylindrical Dimensions with Dissolution Time. The $KHCO_3$ solid was examined after dissolution in DMF at elevated temperatures to gain insight into the changes in the cylindrical particle sizes with dissolution time. A solution of DMF with $KHCO_3$ of mass 1.00 g was heated under ultrasound at 100 °C with the addition of an excess of 2-cyanophenol, assuming complete dissolution of the solid was possible. The solid was then removed 1 h after the 2-cyanophenol addition, dried under vacuum ,and analyzed by SEM. Figure 8 shows an image of the $KHCO_3$ after the dissolution time of 1 h. From examination of the images, the mean cylindrical particle dimensions were estimated to be $d = 145 \pm 110$ μm, $l = 310 \pm 260$ μm, and ratio $z = 2.2 \pm 0.5$. A comparison to the mean initial particle dimension of the $KHCO_3$ sample indicates an approximate decrease in d and l of 25 and 80 μm, respectively, and z remains relatively unchanged during the dissolution.

From the developed theory for the dissolution of cylindrical particles, the changes of d and l with dissolution time can be predicted. Utilizing eqs 7 and 8 for a single $KHCO_3$ particle

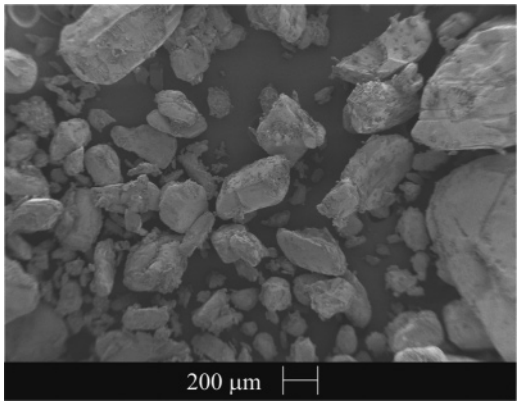

Figure 8. SEM image of $KHCO_3$ after a dissolution time of 1 h in DMF at 100 °C.

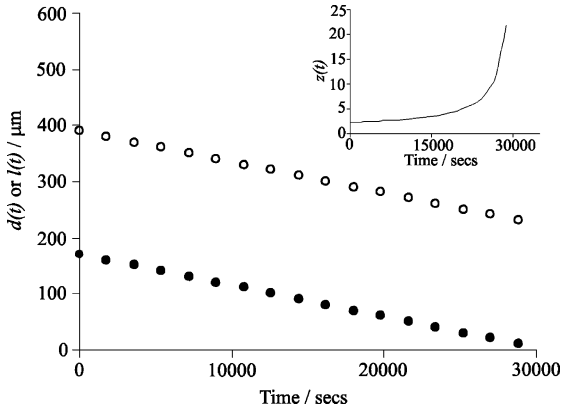

Figure 9. Plots of $d(t)/\mu$m and $l(t)/\mu$m against time/s for the dissolution of a cylindrical $KHCO_3$ particle with $d_0 = 170$ μm and $l_0 = 390$ μm. The inset shows a graph of $z(t)$ against time/s for the dissolution.

with a mean initial diameter of 170 μm, a cylindrical length of 390 μm ($z = 2.3$), and a dissolution rate constant of 6.0×10^{-9} mol cm^{-2} s^{-1}, we yield the plots in Figure 9. Both d and l decrease over time by the same rate of 5.5×10^{-7} cm s^{-1}, calculated from eqs 5 and 6. Complete dissolution of the particle occurs when d becomes zero, at a time of 30 704 s. The inset of Figure 9 shows the change of z ratio with dissolution time, given by eq 9. Because $l_0 \geq d_0$, this ratio increases to infinity as the particle approaches complete dissolution.

After a dissolution time of 1 h, theory predicts that d and l for the $KHCO_3$ cylindrical particle will decrease to values of 150 and 370 μm, respectively, and a z ratio of 2.5. These values compare favorably to the mean values obtained experimentally for the dissolution of $KHCO_3$ in DMF, with a decrease in both dimensions of the same order and little change of z ratio after the 1-h time period.

4.2.4. Investigation of Another $KHCO_3$ Sample. We further tested the model for the surface-controlled dissolution of cylindrical particles by considering another sample of $KHCO_3$, labeled $KHCO_3$*. The dissolution of $KHCO_3$*, composed of cylindrical particles with smaller dimensions and hence different $f(d)$, $f(l)$, and z values (given in Section 4.1.) to those of the prior solid, was followed by the titration of dissolved solid with 2-cyanophenol. Solutions of DMF with $KHCO_3$* of masses 0.025, 0.034, and 0.051 g were heated under ultrasound at 100 °C, with the addition of an excess of 2-cyanophenol, assuming complete dissolution of the solid was possible. Again, the experimental plots of $n(t)$ against time were compared to those generated from the theory, incorporating the cylindrical particle diameter number distribution function, $f(d)$, for $KHCO_3$* (Figure 5b) and assuming the mean z_0 value of 2.6 for all

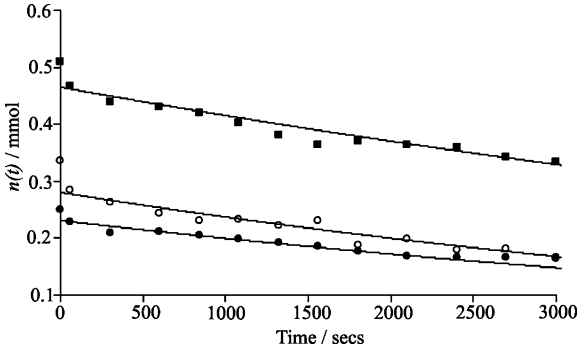

Figure 10. Plots of $n(t)$/mmol against time/s of theoretical results from the cylinder model (−) and UV/visible spectroscopic experimental results at 100 °C for the dissolution-rate-controlled process of (●) 0.025 g $KHCO_3$*, (○) 0.034 g $KHCO_3$*, and (■) 0.051 g $KHCO_3$*.

particles. The results are detailed in Figure 10 and good data fits are observed, from which the mean value determined for the dissolution rate constant, k, for the dissolution of $KHCO_3$* in DMF at 100 °C is $(8.9 \pm 1.3) \times 10^{-9}$ mol cm^{-2} s^{-1}. This value is in excellent concurrence with that found for the dissolution at 100 °C of the previous sample of $KHCO_3$ (Table 1). We have shown successfully that the surface-controlled dissolution model can be applied to a second inorganic solid sample of cylindrical particles, which is described by a different number distribution function, $f(d)$. The dissolution rate constant, k, for $KHCO_3$ at 100 °C is independent of the initial sizes of the cylindrical particles, hence supporting the dissolution model.

5. Conclusions

We present a theoretical model for the surface-controlled dissolution of cylindrical solid particles for a monodispersed solid and for that where the cylindrical size distribution of all particles in the solid is known. A comparison of this to previous theory for spherical particles emphasizes the importance of knowing the shapes of the individual solid particles when modeling the dissolution kinetics.

The surface-controlled dissolution of cylindrical particles model was employed to interpret experimental data published previously for the dissolution of $KHCO_3$ in DMF at elevated temperatures. SEM images of the $KHCO_3$ sample revealed that the particles were much more cylindrical in shape, and not spherical as might be niavely assumed. It was found that the cylindrical model gave improved fits over all of the experimental results. From this refinement, the dissolution rate constant, k, for $KHCO_3$ was determined to be $(9.6 \pm 1.6) \times 10^{-9}$ mol cm^{-2} s^{-1} at 100 °C and the activation energy for the dissolution was 34.5 kJ mol^{-1} over the temperature range of 60−100 °C investigated. The model was then applied successfully to the dissolution in DMF of another sample of $KHCO_3$ comprised of cylindrical particles with a different number distribution function, $f(d)$, to produce a particle size and shape independent value for the dissolution rate constant.

Acknowledgment. C.L.F. expresses her gratitude to the EPSRC for a DTA studentship and Syngenta for a CASE award. We also thank Syngenta for the use of their facilities for carrying out the Karl Fischer titrations. O.V.K. thanks the Clarendon Fund for partial support.

References and Notes

(1) Booth, J.; Sanders, G. S. H. W.; Compton, R. G.; Atherton, J. H.; Brennan, C. M. *J. Electroanal. Chem.* **1997**, *440*, 83.

(2) Yartasi, A.; Kocakerim, M. M.; Ozmetin, C.; Abali, Y. *Miner. Eng.* **1996**, *9*, 1269.
(3) Yartasi, A.; Kocakerim, M. M.; Yapici, S.; Ozmetin, C. *Ind. Eng. Chem. Res.* **1994**, *33*, 2220.
(4) Ozbek, H.; Abali, Y.; Colak, S.; Ceyhum, I.; Karagolge, Z. *Hydrometallurgy* **1999**, *51*, 173.
(5) Compton, R. G.; Harding, M. S.; Pluck, M. R. *J. Phys. Chem.* **1993**, *97*, 10416.
(6) Abali, Y.; Colak, S.; Yartasi, A. *Hydrometallurgy* **1997**, *46*, 13.
(7) Kunkul, A.; Demirkiran, N.; Baysar, A. *Ind. Eng. Chem. Res.* **2003**, *42*, 982.
(8) Welford, P. J.; Brookes, B. A.; Wadhawan, J. D.; McPeak, H. B.; Hahn, C. E. W.; Compton, R. G. *J. Phys. Chem. B* **2001**, *105*, 5253.
(9) Compton, R. G.; Daly, P. J. *J. Colloid Interface Sci.* **1984**, *101*, 159.
(10) Sanders, G. S. H. W.; Booth, J.; Compton, R. G. *Langmuir* **1997**, *13*, 3.
(11) Tam, K. Y.; Compton, R. G.; Atherton, J. H.; Brennan, C. M.; Docherty, J. H. *J. Am. Chem. Soc.* **1996**, *118*, 4419.
(12) Jeschke, A. A.; Vosbech, K.; Dreybrodt, W. *Geochim. Acta* **2001**, *65*, 27.
(13) Pokrovsky, O. S.; Schott, J. *Environ. Sci. Technol.* **2002**, *36*, 426.
(14) *Research in Chemical Kinetics*; Compton, R. G., Hancock, G., Eds.; Blackwell Science: Oxford, 1997; Vol. 4.
(15) Temur, H.; Yartasi, A.; Copur, M.; Kocakerim, M. M. *Ind. Eng. Chem. Res.* **2000**, *39*, 4114.
(16) Compton, R. G.; Pritchard, K. L.; Unwin, P. R. *Freshwater Biol.* **1989**, *22*, 285.
(17) Allers, T.; Luckas, M.; Schmidt, K. G. *Chem. Eng. Technol.* **2003**, *26*, 11.
(18) Allers, T.; Luckas, M.; Schmidt, K. G. *Chem. Eng. Technol.* **2003**, *26*, 12.
(19) Wilkins, S. J.; Compton, R. G.; Viles, H. A. *J. Colloid Interface Sci.* **2001**, *242*, 378.
(20) Hong, Q.; Suarez, M. F.; Coles, B. A.; Compton, R. G. *J. Phys. Chem. B* **1997**, *101*, 5557.
(21) Borredon, E.; Clavellinas, F.; Delmas, M.; Gaset, A.; Sinisterra, J. V. *J. Org. Chem.* **1990**, *55*, 501.
(22) Bentley, T. W.; Jones, R. V. H.; Larder, A. H.; Lock, S. J. *J. Chem. Soc., Chem. Commun.* **1994**, *19*, 2309.
(23) Albanese, D.; Landini, D.; Maia, A.; Penso, M. *J. Mol. Catal. A: Chem.* **1999**, *150*, 113.
(24) Landini, D.; Penso, M. *J. Org. Chem.* **1991**, *56*, 420.
(25) Custers, J. P. A.; Hersmis, M. C.; Meuldijk, J.; Vekemans, J. A. J. M.; Hulshof, L. A. *Org. Process Res. Dev.* **2002**, *6*.
(26) Fedorynski, M.; Wojciechowski, K.; Matacz, Z.; Makosza, M. *J. Org. Chem.* **1978**, *43*, 4682.
(27) Forryan, C. L.; Klymenko, O. V.; Brennan, C. M.; Compton, R. G. *J. Phys. Chem. B* **2005**, *109*, 2862.
(28) Forryan, C. L.; Klymenko, O. V.; Brennan, C. M.; Compton, R. G. *J. Phys. Chem. B* **2005**, *109*, 8263.
(29) Meyer, A. S., Jr.; Boyd, C. M. *Anal. Chem.* **1959**, *31*, 1.
(30) Banks, C. E.; Compton, R. G. *ChemPhysChem* **2003**, *4*, 169.
(31) Margulis, M. A.; Mal'tsev, A. N. *Russ. J. Phys. Chem.* **1969**, *43*, 592.
(32) Moorcroft, M. J.; Lawrence, N. S.; Coles, B. A.; Compton, R. G.; Trevani, L. N. *J. Electroanal. Chem.* **2001**, *506*, 28.
(33) Forryan, C. L.; Wain, A. J.; Brennan, C. M.; Compton, R. G. *Phys. Chem. Chem. Phys.* **2004**, *6*, 2989.
(34) Harwood, L. M.; Moody, C. J. *Experimental Organic Chemistry: Principles and Practice*; Blackwell Scientific Publications: Oxford, 1989.